




Review

Recent Advances in Carbon Nanotube Technology: Bridging the Gap from Fundamental Science to Wide Applications

Zhizhi Tao ^{1,2}, Yuqiong Zhao ^{1,2}, Ying Wang ^{1,2,*} and Guojie Zhang ^{1,2,*} 

¹ State Key Laboratory of Clean and Efficient Coal Utilization, Taiyuan University of Technology, Taiyuan 030024, China

² Key Laboratory of Coal Science and Technology, Ministry of Education, Taiyuan University of Technology, Taiyuan 030024, China

* Correspondence: zhangguojie@tyut.edu.cn

Abstract: Carbon nanotubes, as carbon allotropes distinguished by their intricate structures and exceptional physicochemical properties, have demonstrated substantial progress in recent years across diverse domains, including energy production, chemical synthesis, and environmental preservation. They exhibit notable attributes such as high thermal stability, superior adsorption capacity, and a substantial specific surface area, rendering them superb catalyst supports. Particularly in electrochemical energy storage, CNTs are extensively employed in supercapacitor electrodes owing to their elevated electrical conductivity, mechanical robustness, and electrocatalytic prowess, which facilitate significant energy storage capabilities. Their intricate pore architecture and reactive sites make functionalized carbon nanotubes well suited for synthesizing composite materials with diverse components, which are ideal for sequestering carbon dioxide from both atmospheric and indoor environments. This review presents a comprehensive examination of carbon nanotube synthesis methodologies, encompassing chemical vapor deposition, arc discharge, and laser ablation, and evaluates their impacts on the structural and functional properties of carbon nanotubes. Furthermore, this article underscores the applications of carbon nanotubes in fields such as fuel cells, photocatalysis, ammonia synthesis, dry methane reforming, Fischer–Tropsch synthesis, and supercapacitors. Despite the considerable potential of carbon nanotubes, their manufacturing processes remain intricate and costly, impeding large-scale industrial production. This review concludes by addressing the challenges in fabricating carbon nanotube composites and outlining future development prospects.

Keywords: carbon nanotubes; applications; industries; materials science; nanotechnology



Citation: Tao, Z.; Zhao, Y.; Wang, Y.; Zhang, G. Recent Advances in Carbon Nanotube Technology: Bridging the Gap from Fundamental Science to Wide Applications. *C* **2024**, *10*, 69. <https://doi.org/10.3390/c10030069>

Academic Editor: Jandro L. Abot

Received: 28 June 2024

Revised: 26 July 2024

Accepted: 31 July 2024

Published: 6 August 2024



Copyright: © 2024 by the authors. Licensee MDPI, Basel, Switzerland. This article is an open access article distributed under the terms and conditions of the Creative Commons Attribution (CC BY) license (<https://creativecommons.org/licenses/by/4.0/>).

1. Introduction

Since the onset of the 21st century, amidst rapid economic expansion and burgeoning population growth, issues pertaining to energy and the environment have garnered increasing prominence [1]. Despite concerted efforts to advocate for clean energy, society remains heavily reliant on fossil fuels, posing a significant threat to sustainable development [2–4]. The combustion of fossil fuels releases greenhouse gases such as carbon dioxide, precipitating a pronounced greenhouse effect [5,6]. Industrial, agricultural, and urban wastewater harbors elevated concentrations of heavy metal ions, organic substances, and microorganisms. Historically, neglecting wastewater treatment has resulted in widespread contamination of global water sources, profoundly impacting access to potable water and human well-being [7]. Nations worldwide are endeavoring to advance cleaner energy conversion, optimize energy efficiency, and implement robust ecological and environmental stewardship. Scientists are addressing these challenges through diverse approaches spanning various disciplines [8]. Scholars from various fields favor carbon and its derivatives due to their diverse surface functional groups, affordability, accessibility, ample pore structures, and distinctive physicochemical properties [9,10]. Carbon nanotubes, an allotrope of

carbon, are esteemed for their elevated specific surface area, electrical conductivity, hollow configuration, hydrophobic nature, abundant surface imperfections, and exceptional mechanical characteristics. They are utilized in chemical synthesis, supercapacitors, water purification, and carbon sequestration [11–14].

Japanese scientist Iijima first observed carbon nanotubes using an electron microscope in 1991 [15]. Carbon atoms within these structures are predominantly sp^2 -hybridized, with the hexagonal lattice exhibiting some degree of curvature that gives rise to a spatial topology. This curvature facilitates the formation of sp^3 -hybridized bonds to varying degrees, resulting in a hybridization state that combines sp^2 and sp^3 characteristics. The overlapping p orbitals extending beyond the graphene layers of carbon nanotubes create highly delocalized π -bonds. These π -bonds on the outer surface of carbon nanotubes provide the chemical foundation for their interaction with conjugated macromolecules via non-covalent bonds [16]. CNTs are seamless hollow cylinders composed of graphene sheets arranged in layers and helically curled at specific angles. They are categorized into single-walled carbon nanotubes (SWCNTs) and multi-walled carbon nanotubes (MWCNTs) based on the number of graphene layers. Titirici et al. [17] utilized photoelectron spectroscopy to demonstrate the presence of distinct functional groups on the surfaces of both SWCNTs and MWCNTs. They proposed that variations in synthesis methods and subsequent treatments result in diverse surface structures in carbon nanotubes. During the formation of MWCNTs, the layers can act as trap centers, leading to the entrapment of various defects, resulting in numerous small, hole-like imperfections in the tube walls. In contrast, SWCNTs typically exhibit a purer surface with fewer defects and greater uniformity compared to MWCNTs. This disparity in surface morphology renders SWCNTs generally more chemically inert than MWCNTs, which are more reactive due to the presence of numerous surface functional groups, such as carboxyl groups.

2. Preparation Methods of Common Carbon Nanotubes

Carbon nanotubes are one-dimensional carbon nanomaterials [18], commonly synthesized via techniques including chemical vapor deposition [19], arc discharge [20], and laser ablation [21]. The resultant structures and properties of these nanotubes vary significantly depending on factors such as the carbon source, heating rate, and catalyst employed in their preparation.

2.1. Chemical Vapor Deposition Method

Chemical vapor deposition (CVD) is utilized to fabricate carbon nanotubes by decomposing carbon-containing gases or vapors as precursor substances at elevated temperatures, facilitating the deposition of carbon atoms. CVD is commonly employed for synthesizing carbon nanotubes from hydrocarbons or alcohols [22]. Kumar et al. [23] introduced an innovative CVD approach using camphor instead of gaseous hydrocarbons. Camphor, a natural substance, aligns with environmentally sustainable and eco-friendly chemical principles. Typical substrate materials utilized for synthesizing carbon nanotubes (CNTs) via chemical vapor deposition include quartz, zeolite, and alloy plates [23,24]. Yamagiwa et al. [25] processed carbon fiber-based substrates by immersing them in dispersions of zirconia nanoparticles at various concentrations for 24 h, followed by vacuum drying. Carbon nanotubes were successfully synthesized in an argon atmosphere using camphor as the carbon source and ferrocene as the catalyst in the vapor deposition process. Energy-dispersive X-ray spectroscopy (EDX) images illustrate that treating carbon fiber substrates with an optimal concentration of zirconia nanodispersion enhances iron nanoparticle formation. This treatment also mitigates premature iron atom formation during precursor pyrolysis, thereby facilitating the effective catalysis of carbon nanotube growth in the vapor phase deposition process. Ha's team [26] initially proposed utilizing ion sputtering-assisted chemical vapor deposition and one-step annealing to transform graphene quantum dots (GQDs) into high-purity graphene and carbon nanotubes adorned with platinum nanoparticles at their tips (Figure 1). Initially, platinum ions are deposited via magnetron sputtering onto

polished silicon wafers, which are subsequently annealed, resulting in the dehydration and aggregation of the platinum films into nanoparticles. These Pt nanoparticles then catalyze the generation of carbon isomers. The team systematically investigated the factors influencing the size, structure, and morphology of these carbon isomers, identifying three pivotal parameters: catalytic ion dose (D), carbon source quantity (S), and thermal energy (T). Their investigation reveals that controlling the evolution from QGDs to CNTs correlates positively with catalytic ion dose (D) and carbon source quantity (S) while correlating negatively with thermal energy (T). This synthesis methodology introduces innovative approaches for fabricating high-purity graphene quantum dot carbon nanotubes.

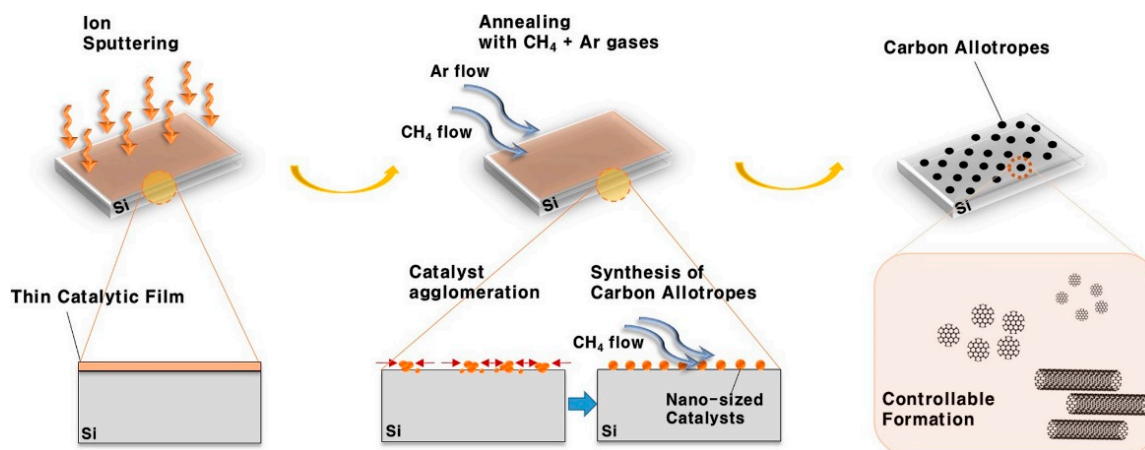


Figure 1. Schematic diagram of ion sputtering-assisted chemical vapor deposition method [26].

2.2. Arc Discharge Method

In 1991, Iijima pioneered the synthesis of carbon nanotubes using the arc discharge method. Subsequently, researchers globally have explored the variables affecting this synthesis approach. This method entails establishing a high-temperature environment via arc discharge between two graphite electrodes. The graphite at the anode evaporates into ionized gaseous species, which subsequently deposit at the cathode, facilitating the formation of carbon nanotubes. Typically, this procedure is conducted under an inert gas atmosphere to inhibit oxidation of the carbon nanotubes. Du et al. [27] demonstrated that varying concentrations of carbon dioxide buffer gas can regulate the length and bundle size of synthesized single-walled carbon nanotubes, effectively removing amorphous carbon from the resulting products. Cai et al. [28] engineered vertical arrays of bamboo-like carbon nanotubes from high-purity graphite carbon powder without employing metallic additives. Takizawa et al. [29] controlled the size distribution of single-walled carbon nanotubes by manipulating Ni/Y ratios in bimetallic catalysts, observing that Ni exerted minimal influence on the nanotubes' diameter. Zhou et al. [30] synthesized pristine multi-walled carbon nanotubes under a nitrogen atmosphere utilizing high-purity graphite powder as the carbon feedstock and iron as the catalyst. They investigated the influence of nitrogen pressure on the structural characteristics of multi-walled carbon nanotubes, observing that higher nitrogen pressure led to elongated nanotubes with reduced curvature. The experimental findings additionally suggest that iron effectively rectifies imperfections in multi-walled carbon nanotubes, presenting a straightforward and cost-effective method for achieving flawless lattice structures. Mehdi's team [31] augmented the yield of multi-walled carbon nanotubes by utilizing an external magnetic field in the arc chamber. They employed thermal purification methods to refine the purity and crystallinity of the nanotubes. Experimental findings illustrate that the application of an appropriately strong unidirectional magnetic field can yield high-purity MWCNTs without substantially altering their tube size distribution. Shifa et al. [32] effectively synthesized multi-walled carbon nanotubes utilizing distilled water as a protective medium. Nevertheless, the resulting product

exhibited impurities including amorphous carbon and other carbonaceous substances, necessitating subsequent purification steps [33].

2.3. Laser Ablation Method

Laser ablation employs a high-energy density laser to transiently heat a designated graphite target, inducing its evaporation into carbon atoms or clusters. Subsequently, these entities are conveyed by an inert carrier gas to a collector located in a cryogenic environment to facilitate carbon nanotube synthesis. In this approach, the carrier gas typically operates under inert atmosphere or vacuum conditions to mitigate oxidation or unfavorable side reactions during the growth of carbon nanotubes. Thess et al. [34] and Rao et al. [35] synthesized single-walled carbon nanotubes employing a dual-beam laser system, enabling control over the nanotube diameter. Alexandrescu et al. [36] synthesized multi-walled carbon nanotubes catalyzed by carbonyl iron particles using CO₂ laser-assisted vapor deposition. A medium-power continuous-wave CO₂ laser irradiated a sensitized mixture of carbonyl iron vapors and acetylene. Concurrently, a silicon substrate was heated to facilitate the growth of carbon nanotubes with diverse morphologies, including single-walled carbon nanotubes. Zhao et al. [37] optimized laser focusing and exploited the interaction between carbon nanotubes and laser irradiation to produce nanoconical arrays of carbon nanotubes. Laser evaporation is used to pattern carbon nanotube films, creating tapered structures. These configurations augment electron emission efficiency and stability, thereby offering potential advantages for applications, such as displays, sensors, and vacuum electronics. Altowyan et al. [38] functionalized multi-walled carbon nanotubes via bis-acid oxidation, followed by the synthesis of NiO-MWCNTs using pulsed laser ablation in liquid (PLAL). Experimental findings evidenced the effective incorporation of NiO into the carbon nanotubes, enhancing interaction capabilities. NiO-MWCNTs demonstrated exceptional efficacy in decomposing methylene blue dye in aqueous solutions, presenting a novel strategy to mitigate challenges in water pollution and wastewater treatment.

3. Carbon Nanotube Applications

3.1. Fuel Cells

Carbon nanotubes demonstrate superb electrical conductivity, mechanical robustness, and chemical stability. These characteristics enable CNT-based electrodes to sustain high conductivity levels and prolong operational longevity in fuel cell environments. Devrim et al. [39] investigated the impact of the graphitization degree on carbon nanotube carriers using microwave-assisted synthesis to deposit platinum on both carbon nanotubes and graphitized carbon nanotubes (GCNTs). They demonstrated that surface oxygen-containing functional groups (-COOH, -OH, etc.) influence the anchoring of platinum nanoparticles, as characterized by techniques, such as TEM. This results in enhanced dispersion of platinum nanoparticles with a reduced average particle size. The experimental results indicate that the Pt/GCNT catalyst displays superior electrochemical performance, stability, and catalytic activity. These benefits are attributed to the graphitic structure, which facilitates rapid electron transfer and strengthens the interaction between platinum and graphitized carbon nanotubes. Wu et al. [40] synthesized an Fe/N/C catalyst derived from metal-organic frameworks (MOFs), which underwent crosslinking with carbon nanotubes. They employed high-temperature ball milling to restructure MIL-53 and ZIF-8, thereby controlling the morphology of the resultant carbon nanotubes through varying the ratio of these two substances. Experimental findings indicated that carbon nanotubes did not form when the MIL-53:ZIF-8 ratio was 1. At ratios of MIL-53:ZIF-8 = 5 or 20, fewer carbon nanotubes were observed, characterized by a short and stout morphology. The crosslinking effect of carbon nanotubes is evidenced in the modification of partially interconnected frameworks, establishing pathways for electron transport and ensuring efficient electron transfer, thereby enhancing oxygen reduction properties. Wang et al. [41] proposed the synthesis of nitrogen-doped carbon nanotubes on carbon fiber cloth surfaces and the fabrication of Pt-CoFe@NCNT/CFC as an electrode material. This was achieved

through the deposition of platinum nanoparticles onto CoFe@NCNT/CFC surfaces using DC plasma magnetron sputtering. Traditional electrodes often involve bonding catalyst particles with adhesives, leading to extensive coverage of active sites and increased charge transfer resistance. Utilizing ion sputtering technology minimizes the quantity of platinum metal used while ensuring uniform distribution on the carbon fiber cloth, thereby markedly improving platinum utilization efficiency. Experimental results demonstrate that Pt-CoFe@NCNT/CFC exhibits robust surface stability as a cathodic catalyst, attributed to nitrogen-doped carbon nanotubes that limit metal exposure to the electrolyte solution, thus preventing direct contact. Bhunia et al. [42] synthesized a cathode material for a methane fuel cell devoid of platinum metal. They prepared Co-g-C₃N₄ as a precursor using conventional methods, subsequently annealing it in a tube furnace to yield Co@NC. The researchers investigated the impact of the annealing temperature on the morphology of Co@NC, observing that higher temperatures resulted in larger carbon nanotubes with thicker wall structures. Experimental observations using FE-SEM revealed spherical Pt nanoparticles uniformly dispersed on the surface of Co@NC, significantly enhancing methanol oxidation activity. Initially, Co@NC and Pt/C displayed comparable oxygen reduction properties. However, elevated synthesis temperatures were found to decrease the nitrogen doping level in the catalyst, potentially reducing the number of sites available for oxygen adsorption and reduction, thereby compromising its oxygen reduction capabilities. Huang et al. [43] developed an innovative cathode catalyst termed FeNi-NCNT/DrGO, as shown in Figure 2. They initially nitrogen-doped modified carbon nanotubes (NCNTs) and embedded iron-nickel alloy nanoparticles (FeNi) into them. Subsequently, FeNi-NCNT was grafted onto defect-rich reduced graphene oxide (DrGO). The FeNi alloy nanoparticles exhibit exceptional bifunctional activity, efficiently catalyzing both the oxygen reduction reaction (ORR) and the oxygen evolution reaction (OER). Following nitrogen doping, NCNTs acquire favorable electronic conduction properties. The synergistic interplay among these three constituents facilitates rapid electrolyte diffusion and enhances the accommodation of discharged species. This synergy allows FeNi-NCNT/DrGO to demonstrate outstanding electrochemical performance.

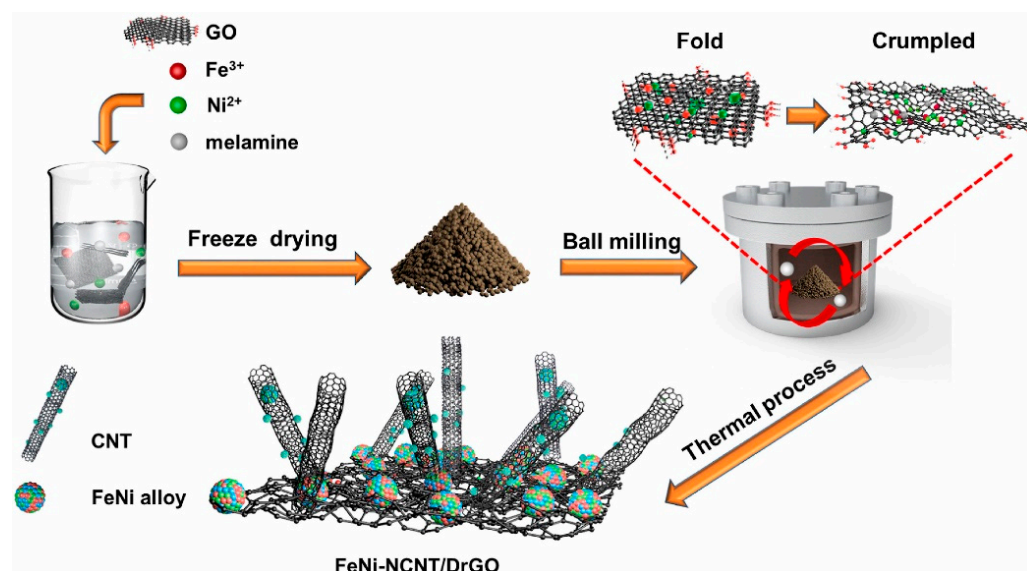


Figure 2. Schematic diagram of FeNi-NCNT/DrGO synthesis [43].

3.2. Photocatalysis

Photocatalytic reactions indeed represent a pivotal pathway for leveraging solar energy, poised to assume growing importance in forthcoming advancements. Whether for sustainable hydrogen production or efficient degradation of waterborne pollutants, this technology holds potential to propel green energy solutions and environmental stewardship

endeavors. Zhou et al. [44] synthesized a metal-free hydrogen evolution photocatalyst via a gas–solid phase reaction involving carbon nanotubes and silicon vapor. The C@SiCNTs were prepared by depositing silicon carbide on the external surface of carbon nanotubes through a gas–solid reaction. The reaction duration and temperature notably influenced the resultant materials. Specifically, extending the reaction time to 4 h resulted in the complete consumption of the carbon nanotubes, leading to the formation of silicon carbide nanotubes (SiCNTs). Alternatively, raising the reaction temperature to 1500 °C resulted in the formation of silicon carbide (SiC) crystals instead of SiCNTs. Compared to CNTs, both C@SiCNTs (carbon-coated silicon carbide nanotubes) and SiCNTs exhibited substantial enhancements in the specific surface area, approximately tripling that of CNTs. Additionally, the average pore size of both C@SiCNTs and SiCNTs is smaller than that of CNTs, enhancing the surface area and pore characteristics. Simulated sunlight experiments demonstrated that among C@SiCNTs, SiCNTs, and SiC, C@SiCNTs exhibited the highest hydrogen evolution performance, highlighting superior photocatalytic activity. After four cycles, hydrogen evolution efficiency remained stable for 20 h, underscoring the robust photocatalytic stability of C@SiCNTs. Bai et al. [45] synthesized a constrained photocatalyst for the degradation of diclofenac using carbon nanotube-constrained perylene diimide. Initially, single-walled carbon nanotubes underwent calcination in a tube furnace to remove end caps. Subsequently, PDA and CNTs were co-processed under vacuum conditions in the same tube furnace. PDA self-assembled onto CNTs at 550 °C, forming PDA@CNT. The lamellar structure of PDA@CNT, as observed in SEM and TEM images, enhances the photocatalytic performance of PDA. The morphology of PDA@CNT is also influenced by the PDA content; for instance, 10PDA@CNT exhibits a more regular tubular structure. Following the stabilization of carbon nanotubes, significant changes in sample morphology are evident. The tubular structure on the surface of PDA@CNT becomes more pronounced, displaying a bamboo-like isotropic structure, indicating the orderly growth of PDA along the CNTs. Electrochemical experiments demonstrate comparable photoresponse intensities for both PDA and PDA@CNT. Furthermore, impedance measurements before and after changing the light source reveal a significant decrease in impedance for PDA@CNT, suggesting enhanced carrier mobility. This confinement effect illustrates the potential of PDA@CNT to improve photocatalytic performance. PDA alone achieved less than 40% degradation of diclofenac, whereas PDA@CNT facilitated the degradation of 97% of diclofenac. Imam's team [46] incorporated molybdenum sulfide as a co-catalyst during the one-pot hydrothermal synthesis of cadmium sulfide photocatalysts using ethylenediamine solvents, successfully anchoring it onto multi-walled carbon nanotubes. The hydrogen production rate and photocatalytic efficiency saw a significant enhancement compared to conditions without a co-catalyst. They attributed this improvement to the formation of heterojunctions involving CdS, carbon nanotubes, and MoS₂. These heterojunctions facilitate efficient charge separation across phases, thereby boosting photocatalytic activity. Experimental findings revealed that optimal loading of carbon nanotubes at 3% led to nearly a sevenfold increase in hydrogen production rates for the composites. Furthermore, the optimal inclusion of MoS₂ at 5% yielded an additional 60% enhancement in hydrogen production performance. Wang et al. [47] introduced cell-like structural photocatalysts featuring phospholipids as an outer membrane coating, as shown in Figure 3. These encapsulated bilayers included Ni-Fe oxides and tin-antimony oxides, with carbon nanotubes integrated into the vesicular structure to function as conduits. The outer phospholipid film and the hydrophobic properties of the carbon nanotubes effectively prevent leaching of the core catalyst in ionic form while facilitating the diffusion of organic molecules into the vesicles for degradation. Moreover, the phospholipid layer encapsulates the toxic semiconductor composite, thereby mitigating the environmental risks associated with its application. This innovation presents promising avenues for semiconductor photocatalysts in environmental remediation applications.

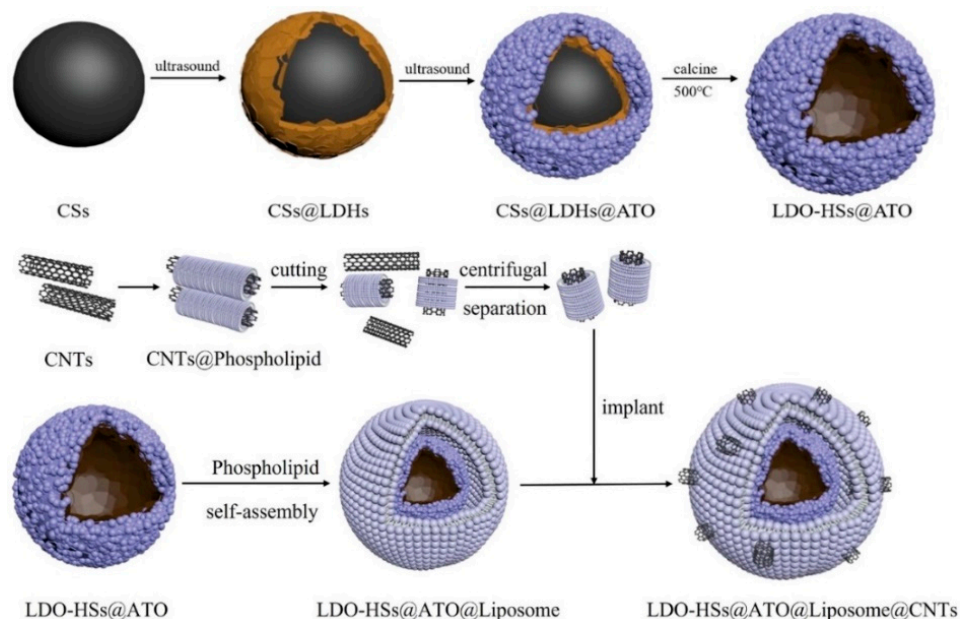


Figure 3. A schematic diagram of the preparation of an artificial vesicular structure photocatalyst [47].

3.3. Ammonia Synthesis

Ammonia synthesis represents a pivotal chemical manufacturing process, with its outputs encompassing diverse applications in agriculture, the chemical industry, medicine, and various other sectors. Ma et al. [48] employed 30% nitric acid for the oxidation of carbon nanotubes, yielding CNTs-O. Subsequently, these were annealed at 850 °C under an argon atmosphere to produce CNTs-D, characterized by a surface rich in defect sites. Barium and ruthenium were sequentially impregnated using a stepwise impregnation method. Ba-Ru/CNTs-D were precipitated with a 30 vol% ammonia solution. Ba-Ru metal was impregnated onto CNTs-O, CNTs-D, and CNTs, respectively. Among these, Ba-Ru/CNTs-D exhibited the highest catalytic activity, achieving a turnover frequency of 0.30 s^{-1} . The experimental findings indicate that ruthenium nanoparticles deposited on defect-rich carbon nanotube surfaces induce a Strong Metal–Support Interaction (SMSI), thereby significantly enhancing catalytic activity and stability during ammonia synthesis. Zhao et al. [49] effectively synthesized a novel Au-CNT catalyst by immobilizing weakly reducing *closo*-[B₁₂H₁₁][−] boron clusters onto the carbon nanotube surfaces, subsequently depositing gold nanoparticles onto this composite support. During the catalytic process converting nitrogen to ammonia, the ammonia production achieved a peak rate of $57.7 \mu\text{g h}^{-1} \text{ cm}^{-2}$, maintaining consistent performance over 18 h of uninterrupted operation. Chen et al. [50] engineered and synthesized a carbon nanotube-supported iron catalyst for electrochemical ammonia synthesis from nitrogen and water under ambient temperature and pressure conditions. This process involves electrolyzing water in one half-cell to provide protons (H⁺) and electrons (e[−]) for hydrogenation, while nitrogen (N₂) undergoes hydrogenation in the other half-cell. Initially, they functionalized carbon nanotubes through nitric acid treatment, introducing diverse oxygen functional groups onto the surface. Subsequently, these functionalized carbon nanotubes were impregnated with iron oxide to form Fe₂O₃-CNT. The catalytic efficiency of Fe₂O₃-CNT surpassed that of previously reported Ru/C catalysts. Nevertheless, it is widely acknowledged that ruthenium demonstrates markedly superior catalytic activity to iron in nitrogen reduction to ammonia. The researchers attributed the heightened activity of Fe₂O₃-CNT to the formation of specific carbon sites at the interfaces between iron nanoparticles and carbon nanotubes, facilitating accelerated N₂ activation and thereby significantly enhancing hydrogenation activity. The absence of precious metals in the catalyst and the simplicity of the preparation method represents substantial strides in the advancement of electrocatalytic water and N₂ ammonia synthesis.

Inspired by molybdenum-containing nitrogenase enzymes found in natural rhizobacteria, Shi et al. [51] synthesized single Mo catalysts (Mo/BCN) by co-doping boron and nitrogen into multi-walled carbon nanotubes, followed by molybdenum loading, as shown in Figure 4. The single Mo atoms are uniformly dispersed on BCN, creating numerous active sites capable of efficiently catalyzing the electrochemical nitrogen reduction reaction. Experimental findings indicated that the highest nitrogen reduction activity was achieved using a 0.1 mol/L potassium hydroxide electrolyte, with a performance yield of $37.67 \mu\text{g h}^{-1} \text{mg}_{\text{cat}}^{-1}$, surpassing that of most noble metal catalysts. Zhang et al. [52] presented findings on a metal-free composite electrocatalyst synthesized at the interface of boron nitride and carbon nanotubes. They explored the impact of incorporating carbon nanotubes on electrocatalytic performance, achieving a peak ammonia yield of $36.5 \mu\text{g h}^{-1} \text{mg}_{\text{cat}}^{-1}$ and a Faraday efficiency of 63.9% with an h-BNN mass ratio of 68.6%. This performance exceeded that of numerous previously reported catalysts. In contrast, standalone h-BNNs exhibited a Faraday efficiency of 4.7%. The notable enhancement in Faraday efficiency was attributed to the formation of C-B and C-N bonds at the interfaces between h-BNNs and CNTs, which were believed to lower the energy barrier of the rate-determining step and improve the selectivity for N_2 -to- NH_3 conversion. After five cycles, the h-BNNs/CNTs composite demonstrated a slight reduction in both ammonia yield and Faraday efficiency, showcasing excellent stability.

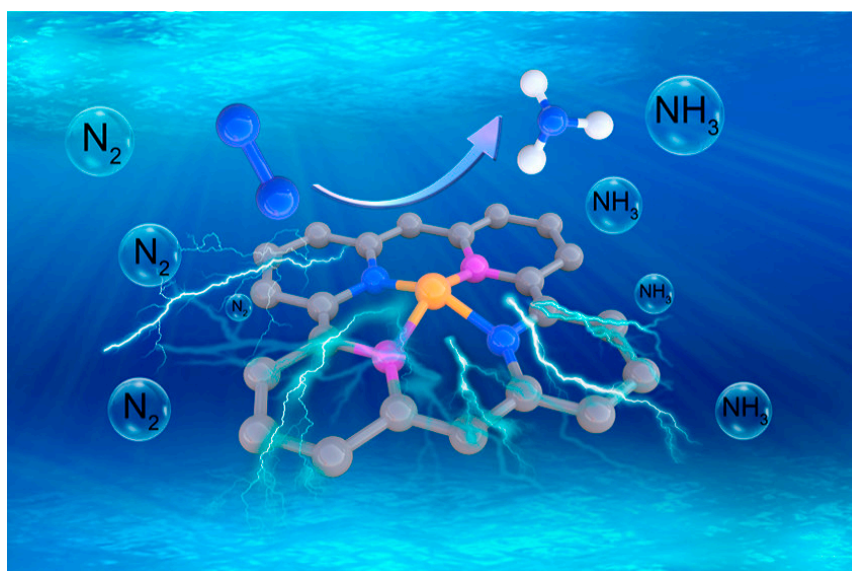


Figure 4. Schematic diagram of Mo/BCN-catalyzed ammonia synthesis mechanism [51].

3.4. Dry Reforming of Methane

The primary advantage of the dry reforming reaction (DRM) of methane lies in its ability to transform two potent greenhouse gases, methane and carbon dioxide, into synthesis gas characterized by a H_2/CO ratio of 1. This synthesis gas is directly applicable in Fischer–Tropsch synthesis processes. Figueira et al. [53] deposited various metals onto both the internal and external surfaces of multi-walled carbon nanotubes (MWCNTs), comparing them with catalysts where the same active metal was loaded either internally or externally. They synthesized CeSr@MWCNT/Co by encapsulating cerium and strontium nanoparticles within the internal cavities of carbon nanotubes while embedding cobalt nanoparticles in the outer walls. To facilitate the deposition of metal particles within the nanotubes, they initially functionalized the carbon nanotubes using nitric acid to introduce oxygen-containing groups and reduce their hydrophobic nature. These modifications ensured the effective deposition of cerium and strontium nanoparticles into the nanotube interiors during synthesis. In methane dry reforming tests, CeSr@MWCNT/Co, loaded with 7 wt.% cerium, 3 wt.% strontium, and 5 wt.% cobalt, exhibited consistent high conversion rates

across various temperatures. The oxygen storage capacity of cerium and the presence of oxygen-containing groups from nitric acid functionalization facilitated oxidation, thereby maintaining a stable H_2/CO ratio in the range of 4.1–5 during the reaction. Kozonoe et al. [54] utilized nitric acid to open the sealed ends of carbon nanotubes, concurrently reducing their hydrophobicity. Subsequently, they introduced nickel nanoparticles into the internal cavities of the carbon nanotubes while depositing iron nanoparticles on the external surfaces. A BET analysis revealed an increase in the specific surface area of the nanotube substrates following nitric acid treatment. The iron deposited on the external surfaces existed as FeO_x , possessing oxidative characteristics that enhanced hydrogen production and improved the catalyst's resistance to carbon deposition. The catalyst $10Ni@CNT/5Fe$ exhibited peak catalytic activity under atmospheric pressure at $800\text{ }^\circ\text{C}$, achieving methane and carbon dioxide conversions of 67% and 88%, respectively. Presently, most fixed-bed reactors used in dry reforming studies employ electric heating. However, temperature gradients from top to bottom reduce energy efficiency. Microwave-assisted heating targets materials that absorb waves directly, offering benefits such as superior heating efficiency, precise temperature control, and rapid response. Traditional metal oxide supports like Al_2O_3 and CeO_2 exhibit limited microwave absorption capabilities. Zhang et al. [55] engineered $Ni@C\text{-}NCNTs$, a material exhibiting exceptional microwave absorption properties and catalytic capability in the dry reforming of methane. Initially, they synthesized Ni-MOF by reacting nickel nitrate hexahydrate with homobenzoic acid, followed by pyrolytic carbonization at $500\text{ }^\circ\text{C}$ to produce $Ni@C\text{-}500$. Compared to its precursor, $Ni@C\text{-}500$ features a rougher surface and a hierarchical structure that largely retains the Ni-MOF morphology, which is crucial for efficient microwave absorption. Subsequently, nitrogen-doped carbon nanotubes were fabricated via annealing in a tube furnace with melamine introduced upstream in the gas stream. This method successfully yielded $Ni@C\text{-}NCNTs$ catalysts with a bilayer core-shell architecture. The dual-layer core-shell configuration mitigates nickel particle agglomeration and enhances catalyst stability. Through comprehensive characterization and theoretical analysis, defects in nitrogen-doped carbon nanotubes were found to accelerate electron transfer, augment methane and carbon dioxide adsorption, and activate catalytic sites, thereby enhancing dry reforming catalytic performance.

3.5. Fischer–Tropsch Synthesis

The Fischer–Tropsch synthesis entails the catalytic conversion of hydrogen and carbon monoxide into liquid hydrocarbons of significant value, with the goal of diminishing reliance on fossil fuels. Nakhaei Pour et al. [56] investigated the impact of solvent magnetization on catalyst morphology and cobalt nanoparticle size during impregnation. They employed a coaxial static magnetic apparatus to magnetize deionized water, subsequently measuring the reduced surface tension of the magnetized water using capillary techniques. Impregnating carbon nanotubes dissolved in magnetized water with cobalt metal resulted in a reduction in the average particle size of cobalt nanoparticles compared to those impregnated in non-magnetized water. The experimental findings demonstrated that catalysts impregnated with magnetized water produced more hydrocarbons and enhanced the likelihood of chain elongation, notably increasing selectivity toward higher hydrocarbons (C^{5+}). Catalysts synthesized from non-magnetized water hindered the formation of long-chain hydrocarbons due to the higher surface tension of deionized water, which predominantly caused cobalt nanoparticles to deposit within the internal cavities of carbon nanotubes. Pendyala et al. [57] investigated the impact of nitric acid treatment on carbon nanotube supports and catalysts synthesized using various preparation methods for Fischer–Tropsch synthesis reactions. Nitric acid treatment serves multiple purposes in modifying carbon nanotubes. It effectively removes surface impurities and introduces additional oxygen-containing functional groups onto the carbon nanotube walls. This process reduces the hydrophobic nature of the nanotubes and facilitates the opening of the closed ends of carbon nanotubes. These apertures provide sites where ruthenium metal particles can be loaded into the interior of the nanotubes. Furthermore, the nitric acid treatment facilitated

the breaking of carbon nanotubes at defect sites. This structural modification shortened the diffusion path for ruthenium nanoparticles, thereby reducing transport resistance. Additionally, the introduced oxygen-containing functional groups played a pivotal role in anchoring ruthenium particles during the deposition process. These combined effects enabled the stable and efficient deposition of ruthenium inside the lumen of carbon nanotubes. In catalysts synthesized via vapor phase deposition, ruthenium nanoparticles typically adhere to the external surface of carbon nanotubes. The lack of confinement within the nanotubes facilitates easier sintering of the active phase. The experimental findings indicated that acid-treated catalysts exhibited heightened catalytic activity and enhanced selectivity toward alcohols and liquid hydrocarbons (C^{5+}) while demonstrating reduced selectivity toward methane. Akbarzadeh et al. [58] investigated the influence of the thermal pretreatment temperature on multi-walled carbon nanotubes subsequent to acid treatment. At a thermal pretreatment temperature of 900 °C, they observed that the proportion of cobalt oxide nanoparticles deposited within the carbon nanotube lumen could reach up to 70%. They reported that Co/CNTs.A.900 achieved a noteworthy 59% conversion of carbon monoxide under conditions of 240 °C and 2.0 MPa. Elevating the temperature to 900 °C enhances the loading of cobalt nanoparticles, thereby augmenting catalytic activity. Thermal pretreatment improves the dispersion of active metals and alters the morphology, structure, and physicochemical properties of the catalysts. Almkhelfe et al. [59] delineated an adapted photo-Fenton process utilized in the fabrication of Fischer–Tropsch synthesis catalysts, as shown in Figure 5. Iron or cobalt hydroxides served as catalyst precursors, with hydrogen peroxide acting as the oxidizing agent. Initially, carbon nanotubes and hydrogen peroxide were amalgamated and agitated at 60 °C, followed by the incremental addition of precursors and oxidants in phases spanning four days. Following the introduction of the initial hydroxide and hydrogen peroxide batch, UV irradiation at a wavelength of 300 nm was administered. The preparation process avoided the introduction of impurities, such as nitrates. Relative to conventional wet impregnation methods, the photo-Fenton approach demonstrated the superior dispersion of active metals, yielding catalyst particles characterized by diminutive and uniform dimensions. Experimental findings underscored the heightened catalytic efficacy of catalysts prepared via the photo-Fenton technique at lower temperatures. Furthermore, metal sintering was mitigated, particularly evident in cobalt-based catalysts, achieving up to 80% CO conversion with robust selectivities toward high-carbon hydrocarbons, typically around 70%. The photo-Fenton method presents an environmentally conscious route for synthesizing Fischer–Tropsch catalysts, obviating the need for calcination during catalyst formulation while upholding superior catalyst durability and high selectivity for carbon monoxide and liquid hydrocarbons.

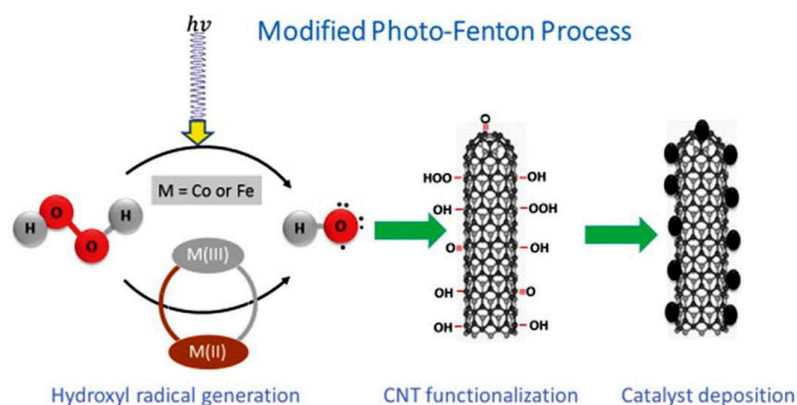


Figure 5. A schematic diagram of the modified light-Fenton method [59].

Zhan et al. [60] engineered and synthesized a hollow polyhedral catalyst (H-Co@NCNHP) comprising nitrogen-doped carbon nanotube housing embedded with hollow cobalt nanoparticles. The synthesis commenced with the ultrasonication of ZIF-67, followed by py-

rolysis in a H₂/Ar atmosphere. Hydrogen facilitated the formation of cobalt nanoparticles, catalyzing the growth of nitrogen-containing nanotubes, resulting in S-Co@NCNHP. The subsequent oxidation in an O₂/Ar atmosphere yielded H-Co₃O₄@NCNHP, followed by a reduction in a H₂/Ar atmosphere to achieve H-Co@NCNHP. Experimental results highlighted that the turnover frequency of H-Co@NCNHP reached up to $1.67 \times 10^{-5} \text{ mol g}_{\text{cat}}^{-1} \text{ s}^{-1}$. Furthermore, the catalyst demonstrated exceptional stability throughout a 120 h durability assessment.

3.6. Supercapacitors

Flexible electronics, incorporating wearable and portable features, represent a promising technology poised to revolutionize our lives in the near future [61–66]. Huang et al. [67] detailed a flexible supercapacitor featuring an aluminum-based vertical array carbon nanotube architecture. Initially, they utilized a laser to etch micro-grooves into the surface of an aluminum substrate. The selection of the laser was guided by a comparative analysis of the electrochemical characteristics of the carbon nanotube structure post-etching, opting for a laser with a power ratio of 1. According to Equations (1) and (2), the surface area of the aluminum foil expanded by a factor of 22 following the etching, leading to a corresponding increase in the specific surface area of the deposited carbon nanotubes. The phase angle of the etched supercapacitor approximates 90°, markedly higher than that of the unetched counterpart (75°), indicating superior charge transfer and ion diffusion properties [68]. Laser-etched vertical array carbon nanotube (VACNT) electrodes exhibit exceptional high-rate performance and capacitance recovery, facilitated by the uninterrupted conductive pathways and distinctive pore structure inherent to VACNTs. Unlike conventional coating methods, directly growing carbon nanotubes on aluminum foil does not obstruct ion and electron transport paths while enhancing the adhesion strength of active materials, thereby enabling rapid charge/discharge capabilities.

$$D = \frac{\pi * d * n * l + (1 - n * \pi * (\frac{d}{2})^2)}{1 * 1} \quad (1)$$

$$n = (\frac{10^4}{d + d_0})^2 \quad (2)$$

where D is the increase factor of the specific surface area after laser etching; *d* and *d*₀ are the etched width and the distance between the microgrids, respectively; *l* is the substrate thickness; and 1 * 1 is the area of the Al microgrid.

Zhu et al. [69] engineered and fabricated a flexible electrode composed of hollow hierarchical porous carbon nanofibers (PANI@HPCNFs) interconnected by CNTs. The outer shell of these nanofibers was fabricated via the electrospinning of polyacrylonitrile (PAN), polymethylmethacrylate (PMMA), and polyvinylpyrrolidone (PVP). The core of these nanofibers consisted of PMMA and MWCNTs, where PMMA functioned as a hollow structure and a mesoporous template. Concurrently, PVP served as a microporous template. This architecture enabled the incorporation of both mesopores and micropores, thereby augmenting the ion storage capacity. Moreover, MWCNTs were incorporated to act as interlayer bridging channels within the electrode architecture. In order to enhance the energy storage capability, the PAN was modified onto the hierarchical porous carbon nanofibers bridged by carbon nanotubes (HPCNFs@CNTs) through an in situ polymerization process. Song et al. [70] proposed an innovative capacitor configuration termed hollow porous carbon-encapsulated carbon nanotubes (CNTs@HPC). The charge storage capability of hollow carbon shells is primarily governed by the surface area available within these structures. While structural alterations can augment the specific surface area of these shells, there exists a practical threshold for the charge storage capacity of a singular component material. Directly encapsulating the secondary component proves more efficient than modifying the structure of the carbon shell itself. The incorporation of carbon nanotubes into capacitor electrodes not only enhances the specific surface area and ion storage capacity but

also improves conductivity, thereby boosting the electron transport rates. Gong et al. [71] proposed a sandwich-structured wood-ceramic electrode composed of bamboo flakes interleaved between bamboo filaments. The bamboo filaments underwent pretreatment in a dilute sodium hydroxide solution followed by boiling, while the thin bamboo flakes were treated with boiling H_3PO_4 for 30 min and subsequently impregnated with cobalt metal using ultrasonication. After impregnation with a phenolic resin solution, the material was hot-pressed into a sandwich structure, with bamboo filaments serving as the central layer and bamboo flakes as the outer layer. Scanning electron micrographs illustrate that the interlaminar bamboo fiber bundles are interconnected, forming a three-dimensional grid structure that facilitates deposition sites for carbon nanotubes. Meanwhile, the longitudinal sections of the bamboo slices preserve their inherent radial arrangement. Bamboo slices without Co/P impregnation exhibit a petal-like morphology under high-magnification scanning electron microscopy. Several varied supercapacitors incorporating carbon nanotubes have been cataloged in Table 1. It was noted that regardless of the energy storage mechanism (electric double-layer capacitor or pseudo-capacitor), their capacitance retention remains approximately 90% even after 5000 cycles or more, showcasing notable stability. In conclusion, we propose that carbon nanotubes exhibit substantial potential for applications in wearable electronics and energy storage sectors.

Table 1. Performance of carbon nanotube and carbon nanotube composite supercapacitors.

Device	Device Type	Substrate	Areal Capacitance [mF cm ⁻²]	Capacitance Retention [Cycles]	References
Laser-etched VACNT electrode	EDLC	Al microgrid	1300	90% (20,000)	[67]
PANI@HPCNFs@CNTs	EDLC	NA	405.2	88.5% (5000)	[69]
CNTs@HPC composite	EDLC	NA	197.09	91% (5000)	[70]
CNT/GNF composite	EDLC	NA	2.16	94.6% (10,000)	[72]
CNT/PC composite	EDLC	NA	300	97% (5000)	[73]
CNT forests	EDLC	SS	5.99	95% (10,000)	[74]
P3MT/HACNT	Pseudo SC	PDMS	3100	92% (5000)	[75]
MnHCF-MnO _x /ErGO	Pseudo SC	PET	16.8	89% (5000)	[76]
PPy(DBS)/CNTs	Pseudo SC	PDMS	3.6	90% (5000)	[77]

HPCNFs: hierarchical porous carbon nanofibers; HPC: hollow porous carbon; GNFs: graphitic nanofibers; HACNT: horizontally aligned carbon nanotube arrays; MnHCF: manganese hexacyanoferrate; ErGO: electrochemically reduced graphene oxide; MnO_x: manganese oxide; PPy (DBS): dodecyl benzene sulfonate-doped poly pyrrole.

3.7. Carbon Capture

In recent years, there has been a notable increase in the atmospheric concentration of carbon dioxide, emerging as a principal reason for global climate change [78–81]. Carbon nanotubes are commonly utilized as robust adsorbents for the capture of carbon dioxide, owing to their extensive specific surface area. Hsan et al. [82] proposed the utilization of bio-waste chitosan-grafted functionalized carbon nanotubes (CSMWCNTs) for the adsorption and immobilization of carbon dioxide under atmospheric conditions. Chitosan, despite its relatively modest specific surface area and limited adsorption efficiency, is being explored for its interaction between surface amine groups and the acidic gas, carbon dioxide. Moreover, CSMWCNTs have demonstrated significant catalytic activity in the chemical immobilization of carbon dioxide with epoxides (such as propylene oxide and

styrene oxide), leading to the formation of cyclic carbonates. An XRD analysis revealed that the characteristic diffraction peaks of carbon nanotubes remained largely unchanged after functionalization, indicating minimal disruption of nanotube symmetry by acid treatment. FT-IR spectroscopy showed increased intensity in the amide group peak, confirming successful grafting of chitosan (-NH₂) onto functionalized multi-walled carbon nanotubes (-COOH), as shown in Figure 6. The specific surface area of CSMWCNTs was enhanced compared to chitosan alone, resulting in improved CO₂ adsorption properties. Additionally, the incorporation of amine and hydroxyl groups effectively mitigated carbon nanotube toxicity. Lee et al. [83] developed a novel category of liquid carbon dioxide adsorbents employing carbon nanotubes and silicone oil. The liquid carbon dioxide adsorbents (LLAs) were formulated utilizing CNTs, renowned for their expansive specific surface area and porous architecture, thereby enhancing the efficacy of carbon dioxide capture. Traditional liquid adsorbents often encounter constraints related to mobility and dispersal in diverse environmental settings. However, the hydrophobic properties of carbon nanotubes and the elevated viscosity of silicone oil mitigate these challenges, amalgamating the advantages of liquid and solid adsorbents. The inherent hydrophobicity of carbon nanotubes safeguards against activity loss from moisture exposure. Additionally, bonding silicone oil to the carbon nanotubes reduces their strength, facilitating their application as a coating. Experimental findings demonstrate that the LLAs exhibit prolonged stability, maintaining CO₂ capture efficiency at 95% even after twenty cycles. Lee et al. [84] engineered a carbon dioxide capture material utilizing carbon nanotubes enveloped in a sodium hydroxide solution, building upon prior research. Initially, they modified the multi-walled carbon nanotubes with octadecylsilane to enhance their lipophilicity, facilitating penetration into silicone oil. This material offers the distinct advantage of recovering the oil phase after separating water of crystallization. The adsorption capacities were quantified at 2.23 mmol/g_{ES-NaOH}⁻¹ in pure CO₂ environments and 1.31 mmol/g_{ES-NaOH}⁻¹ in low CO₂ environments at 2000 ppm and 50% relative humidity. The addition of 0.075 wt.% carbon nanotubes resulted in a minimized emulsion droplet size, achieving a CO₂ capture efficiency of 87.6% for ES-NaOH.

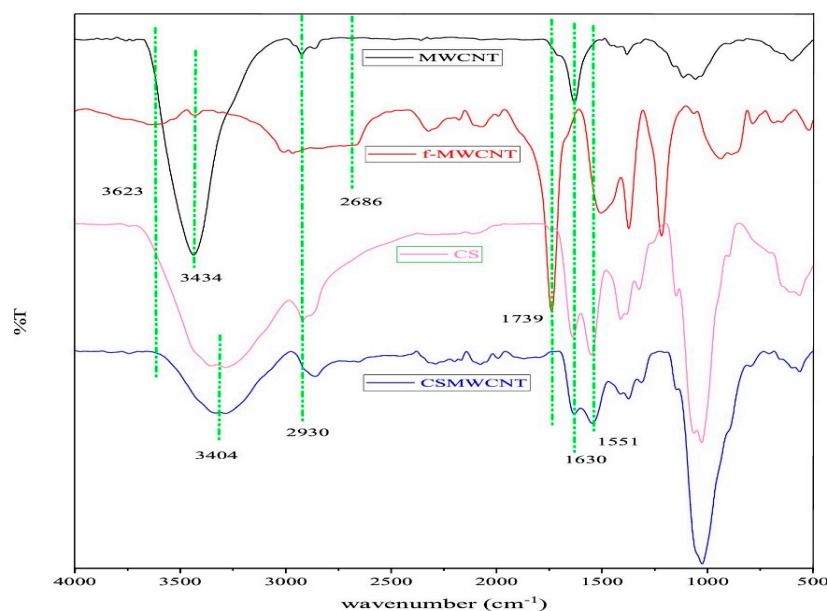


Figure 6. FTIR spectra of MWCNTs, f-MWCNTs, CS, and CS-grafted MWCNTs [82]. Notes: Cs: chitosan.

3.8. Sensor and Biosensors

Carbon nanotubes, owing to their distinctive optical, electrical, and mechanical characteristics, represent excellent candidates for sensor components due to their capacity to enter into a nano-grid and recognize the addition of specific elements. Particularly, single-walled

carbon nanotubes exhibit heightened sensitivity in their transport properties to environmental stimuli. Carbon nanotube biosensors offer rapid and precise analysis of biological metabolites, facilitate the real-time monitoring of biological health and timely disease detection, and thereby bolster contemporary medical interventions. Kim and colleagues developed a single-walled carbon nanotube chemosensor designed for nitrogen dioxide monitoring [85]. They fabricated a single-walled carbon nanotube film without surfactants using aerogel vapor deposition. This process utilizes CO as a carbon source, ferrocene as a catalyst precursor, and CO₂ as a growth promoter for carbon nanotubes, which are formed via CO disproportionation yielding carbon, thereby generating carbon nanotubes. The stability of the carbon monoxide molecule results in a low rate of decomposition, significantly reducing non-catalytic pyrolytic carbon and defects. This method produces carbon nanotubes with few surface defects and a high surface-to-volume ratio and facilitates excellent dispersion without surfactant assistance. Scanning electron microscopy (SEM) images illustrate that aerosolized SWCNTs exhibit a well-defined lattice structure with long bundles and uniform tube diameters compared to conventional solution methods, enhancing the sensor's gas-sensitive performance. Experimental data indicate the sensor achieves a sensitivity of 41.6% at 500 ppb, with response and recovery times of 14.2 and 120.8 s, respectively, and a detection limit as low as 0.161 ppb. In a fine-dust environment, particulate matter covers adsorption sites, slightly diminishing sensor reactivity and prolonging response times yet still enabling effective NO₂ gas monitoring. Kouediatouka et al. [86] devised and fabricated a pressure sensor comprising a PE/CNT/LM/PE configuration, where PE denotes a polydimethylsiloxane (PDMS):Ecoflex blend at a ratio of 2:1 serving as the substrate. Carbon nanotube/liquid metal (CNT/LM) coatings were applied between the two layers of the PE substrate, forming a monolithic sandwich structure. By employing UV laser enhancement to fortify the adhesion of the coatings to the substrate, they bolstered the conductivity of the conductive layer while mitigating the oxidized layer of the liquid metal to sustain optimal conductivity. The CNT/LM blend demonstrated remarkable stability, exhibiting no signs of precipitation or delamination after a two-week period. Rheological assessments revealed that the CNT and LM components were intricately entangled, imparting gel-like properties to the CNT/LM blends, facilitating their stable deposition onto the PE surface. Particle size analyses indicated that the average diameter of CNT/LM blends was smaller compared to individual CNTs and LM, with the CNT/LM solution achieving superior dispersion. Experimental findings demonstrated that the PE/CNT/LM/PE pressure sensors displayed sensitivity and recoverability under varying compressive strains, exhibiting a sensitivity range from 20.6 (at 10% strain) to 57 (at 30% strain) and a rapid response time of 70 ms. Impressively, stability tests over 1000 cycles at 25% strain showcased excellent sensing stability, with a load capacity of up to 2451 N. Feng et al. [87] designed and fabricated a field-effect transistor (FET) device using high-purity carbon nanotubes (CNTs) to capture *Salmonella enterica* (*S. enterica*) and *Staphylococcus aureus* (*S. aureus*). They functionalized the CNT-FET with aptamers specific to the nucleic acids of *S. enterica* and *S. aureus*, enhancing the biosensor's affinity and selectivity toward these pathogens. This modification enabled the CNT-FET biosensor to demonstrate exceptional sensitivity. In phosphate buffer solution (PBS), the CNT-FET biosensor achieved detection limits as low as 1 CFU for *S. enterica* and 1.2 CFUs for *S. aureus*. Even when challenged with six complex food matrices, the biosensor maintained its high sensitivity and rapid response, detecting as few as 3.1 CFUs with a detection time of under 200 s.

4. Challenges and Future Perspectives

Carbon nanotubes, as a novel material with a unique structure and excellent physico-chemical properties, have demonstrated significant application potential in various fields, such as energy production, chemical synthesis, and environmental protection. They exhibit not only high thermal stability, an exceptional adsorption capacity, and a large specific surface area but also outstanding performance as catalyst supports. Particularly in the field

of electrochemical energy storage, carbon nanotubes are widely employed as electrodes in supercapacitors due to their high electrical conductivity, mechanical stability, and electrocatalytic activity, thus showcasing superior storage capacity. Moreover, owing to their rich porous structure and active sites, functionalized carbon nanotubes have been integrated with other materials to develop composite materials suitable for capturing carbon dioxide in atmospheric or indoor environments. These advancements not only highlight the potential of carbon nanotubes in energy production and environmental protection but also offer new perspectives for the advancement of materials science. Despite the broad prospects of carbon nanotubes, their practical applications face numerous challenges.

Firstly, the preparation techniques and cost considerations pose significant challenges in the application of carbon nanotubes. Current methods for synthesizing carbon nanotubes, such as chemical vapor deposition (CVD), laser ablation, and arc discharge, though capable of producing high-quality materials, involve intricate processes and substantial production costs. Particularly in large-scale production, ensuring the consistency and purity of carbon nanotubes while reducing manufacturing costs remains a pressing issue. Presently, most production methods remain at the laboratory stage and have yet to achieve full commercial viability. Therefore, future advancements are imperative to develop more efficient and cost-effective synthesis technologies for widespread industrial and everyday applications.

Secondly, functionalization of carbon nanotubes presents another significant challenge. To meet diverse application needs, carbon nanotubes typically require functional modifications, such as surface modifications or specific element doping. These functional treatments impart new capabilities to carbon nanotubes but may also alter their fundamental properties. For instance, functionalization processes can affect the electrical conductivity and mechanical performance of carbon nanotubes, thereby influencing their performance in specific applications. Hence, precise control over processing conditions is crucial during functionalization to preserve the excellent properties of carbon nanotubes while achieving the desired functionalities. Furthermore, understanding the complex synergistic mechanisms between carbon nanotubes and composite materials remains pivotal for optimizing material performance. Future research efforts should therefore focus on further exploring the nature of interactions between carbon nanotubes and composites, aiming to maximize their performance through adjustments in material composition and structure.

Lastly, environmental and health safety concerns represent significant challenges in the application of carbon nanotubes. Due to their minute dimensions and high surface area, carbon nanotubes may pose potential risks to biological organisms and the environment. Studies have indicated that prolonged exposure or inhalation of carbon nanotubes could adversely affect health, leading to pulmonary diseases and immune system disorders. Moreover, carbon nanotubes are persistent in the environment and may exert long-term impacts on ecosystems due to their poor degradation characteristics. Consequently, future research needs to prioritize investigating the biocompatibility of carbon nanotubes and their environmental impacts to ensure their safe usage and environmental sustainability.

In summary, the prospects for carbon nanotube applications are expansive, accompanied by challenges and opportunities alike. To address these challenges comprehensively, we must proceed on several fronts: Firstly, by intensifying foundational research to delve deeply into the structural–performance relationships of carbon nanotubes, thereby providing theoretical guidance for practical applications. Secondly, by optimizing synthesis processes to enhance the yield, purity, and consistency of carbon nanotubes. Thirdly, by refining dispersion techniques to improve the dispersibility of carbon nanotubes within matrix materials. Fourthly, by prioritizing biosafety considerations to ensure the secure application of carbon nanotubes in biomedical fields. Fifthly, by fostering interdisciplinary collaboration to promote the integration of academia, industry, and research, thereby driving innovation and advancement in carbon nanotube application technologies. Looking forward, with the continuous advancement of scientific research and technology, the challenges in carbon nanotube applications will gradually be overcome. We have reason to believe that in the near future, carbon nanotubes will achieve significant breakthroughs

in electronics, energy, composite materials, biomedical applications, and beyond, ushering unprecedented opportunities for societal development and bolstering the global high-tech industry.

Author Contributions: Conceptualization, Z.T. and G.Z.; methodology, Y.Z.; validation, Y.Z. and Y.W.; formal analysis, Y.Z.; investigation, Z.T.; resources, G.Z.; writing—original draft preparation, Z.T.; writing—review and editing, G.Z.; visualization, Y.Z.; supervision, G.Z.; project administration, Y.W.; funding acquisition, Y.Z., Y.W. and G.Z. All authors have read and agreed to the published version of the manuscript.

Funding: This work was supported by the Applied Basic Research Project of Shanxi Province (Nos. 202303021211032, 202303021211034, and 202203021222130), Key R&D Program of Lvliang (2022GXYF02), and National Natural Science Foundation of China (No. 21878200).

Data Availability Statement: Unavailable due to it being a Review paper.

Acknowledgments: The authors are grateful to the Taiyuan University of Technology for its support.

Conflicts of Interest: The authors declare no conflicts of interest.

References

- Sandru, M.; Sandru, E.M.; Ingram, W.F.; Deng, J.; Stenstad, P.M.; Deng, L.; Spontak, R.J. An integrated materials approach to ultrapermeable and ultrasensitive CO₂ polymer membranes. *Science* **2022**, *376*, 90–94. [[CrossRef](#)]
- Rogelj, J.; Huppmann, D.; Krey, V.; Riahi, K.; Clarke, L.; Gidden, M.; Nicholls, Z.; Meinshausen, M. A new scenario logic for the Paris Agreement long-term temperature goal. *Nature* **2019**, *573*, 357–363. [[CrossRef](#)]
- De Lange, D.E. Climate action now: Energy industry restructuring to accelerate the renewable energy transition. *J. Clean. Prod.* **2024**, *443*, 141018. [[CrossRef](#)]
- Chen, L.; Xu, Q. Fewer defects, better catalysis? *Science* **2020**, *367*, 737. [[CrossRef](#)]
- Ding, X.; Liu, W.; Zhao, J.; Wang, L.; Zou, Z. Photothermal CO₂ Catalysis Towards the Synthesis of Solar fuel: From Material and Reactor Engineering to Techno-Economic Analysis. *Adv. Mater.* **2024**. [[CrossRef](#)]
- Peng, W.; Li, F.; Kong, S.; Guo, C.; Wu, H.; Wang, J.; Shen, Y.; Zhang, M. Recent advances in nickel-based catalysts in eCO₂RR for carbon neutrality. *Carbon Energy* **2024**, *6*, e498. [[CrossRef](#)]
- Mukherjee, A.; Coomar, P.; Sarkar, S.; Johannesson, K.H.; Fryar, A.E.; Schreiber, M.E.; Ahmed, K.M.; Alam, M.A.; Bhattacharya, P.; Bundschuh, J.; et al. Arsenic and other geogenic contaminants in global groundwater. *Nat. Rev. Earth Environ.* **2024**, *5*, 312–328. [[CrossRef](#)]
- Mohammed, S.; Eljack, F.; Al-Sobhi, S.; Kazi, M.K. A systematic review: The role of emerging carbon capture and conversion technologies for energy transition to clean hydrogen. *J. Clean. Prod.* **2024**, *447*, 141506. [[CrossRef](#)]
- Gong, H.; Chen, S.; Tok, J.B.H.; Bao, Z. An emerging class of carbon materials: Synthesis and applications of carbon flowers. *Matter* **2023**, *6*, 2206–2234. [[CrossRef](#)]
- Xue, W.; Zhao, Z.; Bi, H.; Zhang, B.; Wang, X.; Qiu, J. Insights into the role of oxygen-containing functional groups on carbon surface in water–electricity generation. *Nano Res.* **2024**, *17*, 6645–6653. [[CrossRef](#)]
- Wu, Y.; Zhao, X.; Shang, Y.; Chang, S.; Dai, L.; Cao, A. Application-driven carbon nanotube functional materials. *ACS Nano* **2021**, *15*, 7946–7974. [[CrossRef](#)] [[PubMed](#)]
- Hu, Z.; Sun, X.; Zhang, X.; Jia, X.; Feng, X.; Cui, M.; Gao, E.; Qian, L.; Gao, X.; Zhang, J. Kinetic Modulation of Carbon Nanotube Growth in Direct Spinning for High-Strength Carbon Nanotube Fibers. *J. Am. Chem. Soc.* **2024**, *146*, 11432–11439. [[CrossRef](#)]
- Sehrawat, M.; Singh, V.; Rani, M.; Kalra, C.; Bharadwaj, S.; Rani, R.; Bisht, A.; Singh, B.P. Nano-Welded Carbon Nanotube Sponges for Efficient Oil Spill Remediation. *J. Clean. Prod.* **2024**, *467*, 142841. [[CrossRef](#)]
- Zhang, F.Z.; Liu, X.B.; Yang, C.M.; Chen, G.D.; Meng, Y.; Zhou, H.B.; Zhang, S.H. Insights into robust carbon nanotubes in tribology: From nano to macro. *Mater. Today* **2024**, *74*, 203–234. [[CrossRef](#)]
- Iijima, S. Helical microtubules of graphitic carbon. *Nature* **1991**, *354*, 56–58. [[CrossRef](#)]
- Zhang, J.; Liu, X.; Blume, R.; Zhang, A.; Schlögl, R.; Su, D.S. Surface-modified carbon nanotubes catalyze oxidative dehydrogenation of n-butane. *Science* **2008**, *322*, 73–77. [[CrossRef](#)]
- Titirici, M.M.; White, R.J.; Brun, N.; Budarin, V.L.; Su, D.S.; Del Monte, F.; Clark, J.H.; MacLachlan, M.J. Sustainable carbon materials. *Chem. Soc. Rev.* **2015**, *44*, 250–290. [[CrossRef](#)]
- Lv, X.; Zhang, S.; Wang, J.; Wang, M.; Shan, J.; Zhou, S. Charge controlled capture/release of CH₄ on Nb₂CT_x MXene: A first-principles calculation. *J. Mol. Graph. Model.* **2022**, *110*, 108056. [[CrossRef](#)]
- Shah, K.A.; Tali, B.A. Synthesis of carbon nanotubes by catalytic chemical vapour deposition: A review on carbon sources, catalysts and substrates. *Mater. Sci. Semicond. Process.* **2016**, *41*, 67–82. [[CrossRef](#)]
- Arora, N.; Sharma, N.N. Arc discharge synthesis of carbon nanotubes: Comprehensive review. *Diam. Relat. Mater.* **2014**, *50*, 135–150. [[CrossRef](#)]

21. Vander Wal, R.L.; Berger, G.M.; Ticich, T.M. Carbon nanotube synthesis in a flame using laser ablation for in situ catalyst generation. *Appl. Phys. A* **2003**, *77*, 885–889. [[CrossRef](#)]
22. Hata, K.; Futaba, D.N.; Mizuno, K.; Namai, T.; Yumura, M.; Iijima, S. Water-assisted highly efficient synthesis of impurity-free single-walled carbon nanotubes. *Science* **2004**, *306*, 1362–1364. [[CrossRef](#)] [[PubMed](#)]
23. Kumar, M.; Ando, Y. A simple method of producing aligned carbon nanotubes from an unconventional precursor—Camphor. *Chem. Phys. Lett.* **2003**, *374*, 521–526. [[CrossRef](#)]
24. Yamagiwa, K.; Ayato, Y.; Kuwano, J. Liquid-phase synthesis of highly aligned carbon nanotubes on preheated stainless steel substrates. *Carbon* **2016**, *98*, 225–231. [[CrossRef](#)]
25. Yamagiwa, K.; Goudo, D. Synthesis of carbon nanotubes on carbon fiber substrates: Effects of nanozirconia dispersion on the growth of carbon nanotubes. *Jpn. J. Appl. Phys.* **2023**, *63*, 02SP04. [[CrossRef](#)]
26. Ha, J.M.; Lee, S.H.; Park, D.; Yoon, Y.J.; Yang, I.M.; Seo, J.; Hwang, Y.S.; Lee, C.Y.; Suk, J.K.; Park, J.K. Synthesis mechanism from graphene quantum dots to carbon nanotubes by ion-sputtering assisted chemical vapor deposition. *Discov. Nano* **2024**, *19*, 83. [[CrossRef](#)] [[PubMed](#)]
27. Du, F.; Ma, Y.; Lv, X.; Huang, Y.; Li, F.; Chen, Y. The synthesis of single-walled carbon nanotubes with controlled length and bundle size using the electric arc method. *Carbon* **2006**, *44*, 1327–1330. [[CrossRef](#)]
28. Cai, X.; Cong, H.; Liu, C. Synthesis of vertically-aligned carbon nanotubes without a catalyst by hydrogen arc discharge. *Carbon* **2012**, *50*, 2726–2730. [[CrossRef](#)]
29. Takizawa, M.; Bandow, S.; Yudasaka, M.; Ando, Y.; Shimoyama, H.; Iijima, S. Change of tube diameter distribution of single-wall carbon nanotubes induced by changing the bimetallic ratio of Ni and Y catalysts. *Chem. Phys. Lett.* **2000**, *326*, 351–357. [[CrossRef](#)]
30. Zhou, G.; Wu, H.; Deng, Y.; Miao, R.; Lai, D.; Deng, J.; Zhang, J.; Chen, Q.; Shao, Q.; Shao, C. Synthesis of high-quality multi-walled carbon nanotubes by arc discharge in nitrogen atmosphere. *Vacuum* **2024**, *225*, 113198. [[CrossRef](#)]
31. Mehdi SM, Z.; Abbas, S.Z.; Seo, Y.; Goak, J.C.; Lee, N. Enhancing purity and crystallinity of carbon nanotubes by magnetically assisted arc discharge and thermal purification and their field emission characteristics. *Surf. Interfaces* **2024**, *49*, 104442. [[CrossRef](#)]
32. Shifa, M.; Toor, Z.S.; Tariq, F. Arc discharge synthesis and multistep purification of multiwall carbon nanotubes. *Nano* **2024**, *19*, 2450007. [[CrossRef](#)]
33. Imtiaz, S.; Siddiq, M.; Kausar, A.; Muntha, S.T.; Ambreen, J.; Bibi, I. A review featuring fabrication, properties and applications of carbon nanotubes (CNTs) reinforced polymer and epoxy nanocomposites. *Chin. J. Polym. Sci.* **2018**, *36*, 445–461. [[CrossRef](#)]
34. Thess, A.; Lee, R.; Nikolaev, P.; Dai, H.; Petit, P.; Robert, J.; Xu, C.H.; Lee, Y.H.; Kim, S.G.; Rinzler, A.G.; et al. Crystalline ropes of metallic carbon nanotubes. *Science* **1996**, *273*, 483–487. [[CrossRef](#)] [[PubMed](#)]
35. Rao, A.M.; Richter, E.; Bandow, S.; Chase, B.; Eklund, P.C.; Williams, K.A.; Fang, S.; Subbaswamy, K.R.; Menon, M.; Thess, A.; et al. Diameter-selective Raman scattering from vibrational modes in carbon nanotubes. *Science* **1997**, *275*, 187–191. [[CrossRef](#)] [[PubMed](#)]
36. Alexandrescu, R.; Crunteanu, A.; Morjan, R.E.; Morjan, I.; Rohmund, F.; Falk, L.K.L.; Ledoux, G.; Huisken, F. Synthesis of carbon nanotubes by CO₂-laser-assisted chemical vapour deposition. *Infrared Phys. Technol.* **2003**, *44*, 43–50. [[CrossRef](#)]
37. Zhao, J.; Li, Z.; Cole, M.T.; Wang, A.; Guo, X.; Liu, X.; Lyu, W.; Teng, H.; Qv, Y.; Liu, G.; et al. Nanocone-Shaped Carbon Nanotubes Field-Emitter Array Fabricated by Laser Ablation. *Nanomaterials* **2021**, *11*, 3244. [[CrossRef](#)] [[PubMed](#)]
38. Altowyan, A.S.; Toghan, A.; Ahmed, H.A.; Pashameah, R.A.; Mwafy, E.A.; Alrefaee, S.H.; Mostafa, A.M. Removal of methylene blue dye from aqueous solution using carbon nanotubes decorated by nickel oxide nanoparticles via pulsed laser ablation method. *Radiat. Phys. Chem.* **2022**, *198*, 110268. [[CrossRef](#)]
39. Devrim, Y.; Arica, E.D. Investigation of the effect of graphitized carbon nanotube catalyst support for high temperature PEM fuel cells. *Int. J. Hydrogen Energy* **2020**, *45*, 3609–3617. [[CrossRef](#)]
40. Wu, Y.; Huang, J.; Lin, Z.; Li, L.; Liang, G.; Jin, Y.Q.; Huang, G.; Zhang, H.; Chen, J.; Xie, F.; et al. Fe-N_x doped carbon nanotube as a high efficient cathode catalyst for proton exchange membrane fuel cell. *Chem. Eng. J.* **2021**, *423*, 130241. [[CrossRef](#)]
41. Wang, W.; Jiang, Z.; Tian, X.; Maiyalagan, T.; Jiang, Z.J. Self-standing CoFe embedded nitrogen-doped carbon nanotubes with Pt deposition through direct current plasma magnetron sputtering for direct methanol fuel cells applications. *Carbon* **2023**, *201*, 1068–1080. [[CrossRef](#)]
42. Bhunia, K.; Vijayakumar, E.; Raj NP, M.J.; Bejigo, K.S.; Kesavan, D.; Kim, S.J. Cobalt Nanoparticle-integrated Nitrogen-doped Carbon Nanotube as an Efficient Bifunctional Electrocatalyst for Direct Methanol Fuel Cells. *Chem. Eng. J.* **2023**, *473*, 145028. [[CrossRef](#)]
43. Huang, C.C.; Pourzolfaghar, H.; Huang, C.L.; Liao, C.P.; Li, Y.Y. FeNi nanoalloy-carbon nanotubes on defected graphene as an excellent electrocatalyst for lithium-oxygen batteries. *Carbon* **2024**, *222*, 118973. [[CrossRef](#)]
44. Zhou, X.; Gao, Q.; Yang, S.; Fang, Y. Carbon nanotube@ silicon carbide coaxial heterojunction nanotubes as metal-free photocatalysts for enhanced hydrogen evolution. *Chin. J. Catal.* **2020**, *41*, 62–71. [[CrossRef](#)]
45. Bai, X.; Guo, L.; Jia, T.; Hao, D.; Wang, C.; Li, H.; Zong, R. Perylene diimide growth on both sides of carbon nanotubes for remarkably boosted photocatalytic degradation of diclofenac. *J. Hazard. Mater.* **2022**, *435*, 128992. [[CrossRef](#)] [[PubMed](#)]
46. Imam, M.D.; Badreldin, A.; Kakosimos, K.E.; Al-Hashimi, M.; Abdel-Wahab, A. One-pot synthesis of a CdS–MoS₂/CNTs nanocomposite for photocatalytic hydrogen production under visible light. *Int. J. Hydrogen Energy* **2024**, *51*, 1267–1278. [[CrossRef](#)]

47. Wang, L.; Chen, T.; Cui, Y.; Wu, J.; Zhou, X.; Xu, M.; Liu, Z.; Mao, W.; Zeng, X.; Shen, W.; et al. Rational Design of Environmentally Friendly Carbon Nanotube Embedded Artificial Vesicle-Structured Photocatalysts for Organic Pollutants Degradation. *Adv. Funct. Mater.* **2024**, *34*, 2313653. [[CrossRef](#)]
48. Ma, Y.; Lan, G.; Fu, W.; Lai, Y.; Han, W.; Tang, H.; Liu, H.; Li, Y. Role of surface defects of carbon nanotubes on catalytic performance of barium promoted ruthenium catalyst for ammonia synthesis. *J. Energy Chem.* **2020**, *41*, 79–86. [[CrossRef](#)]
49. Zhao, X.; Yang, Z.; Kuklin, A.V.; Baryshnikov, G.V.; Ågren, H.; Zhou, X.; Zhang, H. Efficient ambient electrocatalytic ammonia synthesis by nanogold triggered via boron clusters combined with carbon nanotubes. *ACS Appl. Mater. Interfaces* **2020**, *12*, 42821–42831. [[CrossRef](#)]
50. Chen, S.; Perathoner, S.; Ampelli, C.; Mebrahtu, C.; Su, D.; Centi, G. Electrocatalytic synthesis of ammonia at room temperature and atmospheric pressure from water and nitrogen on a carbon-nanotube-based electrocatalyst. *Angew. Chem. Int. Ed.* **2017**, *56*, 2699–2703. [[CrossRef](#)]
51. Shi, L.; Bi, S.; Qi, Y.; He, R.; Ren, K.; Zheng, L.; Wang, J.; Ning, G.; Ye, J. Anchoring Mo single-atom sites on B/N co-doped porous carbon nanotubes for electrochemical reduction of N₂ to NH₃. *ACS Catal.* **2022**, *12*, 7655–7663. [[CrossRef](#)]
52. Zhang, M.; Shen, L.; Yu, C.; Li, T.; Bai, S.; Su, Y.; Liu, Z.; Li, Y. Boosting the Faraday Efficiency of Electrochemical Ammonia Synthesis via the Strain Effect Induced by Interfacial Hybrid Formation between BN and Carbon Nanotubes. *ACS Appl. Mater. Interfaces* **2024**, *16*, 8832–8841. [[CrossRef](#)] [[PubMed](#)]
53. Figueira, C.E.; Junior PF, M.; Giudici, R.; Alves, R.M.B.; Schmal, M. Nanoparticles of Ce, Sr, Co in and out the multi-walled carbon nanotubes applied for dry reforming of methane. *Appl. Catal. A Gen.* **2018**, *550*, 297–307. [[CrossRef](#)]
54. Kozonoe, C.E.; Santos, V.M.; Schmal, M. Investigating the stability of Ni and Fe nanoparticle distribution and the MWCNT structure in the dry reforming of methane. *Environ. Sci. Pollut. Res.* **2023**, *30*, 111382–111396. [[CrossRef](#)] [[PubMed](#)]
55. Zhang, M.; Gao, Y.; Mao, Y.; Jin, Y.; Wang, W.; Sun, J.; Song, Z.; Zhao, X. Hierarchical core-shell Ni@C-NCNTs nanocomposites tailored for microwave-induced dry reforming of methane process. *J. Mater. Chem. A* **2023**, *11*, 21908–21926. [[CrossRef](#)]
56. Nakhaei Pour, A.; Karimi, J.; Taghipoor, S.; Gholizadeh, M.; Hashemian, M. Fischer-Tropsch synthesis over CNT-supported cobalt catalyst: Effect of magnetic field. *J. Iran. Chem. Soc.* **2017**, *14*, 1477–1488. [[CrossRef](#)]
57. Pendyala VR, R.; Jacobs, G.; Graham, U.M.; Shafer, W.D.; Martinelli, M.; Kong, L.; Davis, B.H. Fischer-Tropsch synthesis: Influence of acid treatment and preparation method on carbon nanotube supported ruthenium catalysts. *Ind. Eng. Chem. Res.* **2017**, *56*, 6408–6418. [[CrossRef](#)]
58. Akbarzadeh, O.; Mohd Zabidi, N.A.; Abdul Wahab, Y.; Hamizi, N.A.; Chowdhury, Z.Z.; Merican Aljunid Merican, Z.; Ab Rahman, M.; Akhter, S.; Rasouli, E.; Johan, M.R. Effect of cobalt catalyst confinement in carbon nanotubes support on fischer-tropsch synthesis performance. *Symmetry* **2018**, *10*, 572. [[CrossRef](#)]
59. Almkhelfe, H.; Li, X.; Thapa, P.; Hohn, K.L.; Amama, P.B. Carbon nanotube-supported catalysts prepared by a modified photo-Fenton process for Fischer-Tropsch synthesis. *J. Catal.* **2018**, *361*, 278–289. [[CrossRef](#)]
60. Zhan, W.; Wang, Y.; Chen, J.; Li, Y. Boosting the Fischer-Tropsch synthesis performances of cobalt-based catalysts via geometric and electronic engineering: Construction of hollow structures. *Appl. Catal. B Environ.* **2022**, *313*, 121469. [[CrossRef](#)]
61. Wang, B.; Huang, W.; Chi, L.; Al-Hashimi, M.; Marks, T.J.; Facchetti, A. High-k gate dielectrics for emerging flexible and stretchable electronics. *Chem. Rev.* **2018**, *118*, 5690–5754. [[CrossRef](#)] [[PubMed](#)]
62. Wang, C.; Sim, K.; Chen, J.; Kim, H.; Rao, Z.; Li, Y.; Chen, W.; Song, J.; Verduzco, R.; Yu, C. Soft ultrathin electronics innervated adaptive fully soft robots. *Adv. Mater.* **2018**, *30*, 1706695. [[CrossRef](#)] [[PubMed](#)]
63. Zhang, X.; Zhao, Y. Wearable droplet microfluidics. *Sci. Bull.* **2019**, *64*, 1472–1473. [[CrossRef](#)] [[PubMed](#)]
64. Park, C.H.; Lee, S.; Pornoppadol, G.; Nam, Y.S.; Kim, S.H.; Kim, B.J. Microcapsules containing pH-responsive, fluorescent polymer-integrated MoS₂: An effective platform for in situ pH sensing and photothermal heating. *ACS Appl. Mater. Interfaces* **2018**, *10*, 9023–9031. [[CrossRef](#)] [[PubMed](#)]
65. Yang, Y.; Gao, W. Wearable and flexible electronics for continuous molecular monitoring. *Chem. Soc. Rev.* **2019**, *48*, 1465–1491. [[CrossRef](#)] [[PubMed](#)]
66. Cho, Y.; Pak, S.; Lee, Y.G.; Hwang, J.S.; Giraud, P.; An, G.H.; Cha, S. Hybrid smart fiber with spontaneous self-charging mechanism for sustainable wearable electronics. *Adv. Funct. Mater.* **2020**, *30*, 1908479. [[CrossRef](#)]
67. Huang, S.; Du, X.; Li, X.; Ma, M.; Xiong, L. Ultrahigh-Areal Capacitance Flexible Supercapacitors Based on Laser Assisted Construction of Hierarchical Aligned Carbon Nanotubes. *Adv. Funct. Mater.* **2021**, *31*, 2104531. [[CrossRef](#)]
68. Liu, Q.; Zhao, A.; He, X.; Li, Q.; Sun, J.; Lei, Z.; Liu, Z.H. Full-temperature all-solid-state Ti₃C₂T_x/aramid fiber supercapacitor with optimal balance of capacitive performance and flexibility. *Adv. Funct. Mater.* **2021**, *31*, 2010944. [[CrossRef](#)]
69. Zhu, J.; Zhang, Q.; Zhao, Y.; Zhang, R.; Liu, L.; Yu, J. Highly flexible, freestanding supercapacitor electrodes based on hollow hierarchical porous carbon nanofibers bridged by carbon nanotubes. *Chem. Eng. J.* **2022**, *434*, 134662. [[CrossRef](#)]
70. Song, G.; Li, C.; Wang, T.; Lim, K.H.; Hu, F.; Cheng, S.; Hondo, E.; Liu, S.; Kawi, S. Hierarchical hollow carbon particles with encapsulation of carbon nanotubes for high performance supercapacitors. *Small* **2024**, *20*, 2305517. [[CrossRef](#)]
71. Gong, L.; Zeng, R.; Shi, Y.; Yu, M.; Yu, X.; Sun, D. Co/P co-doped bamboo-based woodceramics with a sandwich structure modified by carbon nanotube electrodeposition as supercapacitor electrodes. *Bioresour. Technol.* **2024**, *399*, 130573. [[CrossRef](#)] [[PubMed](#)]
72. Liu, X.; Lai, C.; Xiao, Z.; Zou, S.; Liu, K.; Yin, Y.; Liang, T.; Wu, Z. Superb electrolyte penetration/absorption of three-dimensional porous carbon nanosheets for multifunctional supercapacitor. *ACS Appl. Energy Mater.* **2019**, *2*, 3185–3193. [[CrossRef](#)]

73. Avasthi, P.; Balakrishnan, V. Tuning the wettability of vertically aligned CNT–TiO₂ hybrid electrodes for enhanced supercapacitor performance. *Adv. Mater. Interfaces* **2019**, *6*, 1801842. [[CrossRef](#)]
74. Avasthi, P.; Kumar, A.; Balakrishnan, V. Aligned CNT forests on stainless steel mesh for flexible supercapacitor electrode with high capacitance and power density. *ACS Appl. Nano Mater.* **2019**, *2*, 1484–1495. [[CrossRef](#)]
75. Zhou, Y.; Wang, X.; Acauan, L.; Kalfon-Cohen, E.; Ni, X.; Stein, Y.; Gleason, K.K.; Wardle, B.L. Ultrahigh-areal-capacitance flexible supercapacitor electrodes enabled by conformal P3MT on horizontally aligned carbon-nanotube arrays. *Adv. Mater.* **2019**, *31*, 1901916. [[CrossRef](#)]
76. Liang, J.; Tian, B.; Li, S.; Jiang, C.; Wu, W. All-printed MnHCF-MnO_x-based high-performance flexible supercapacitors. *Adv. Energy Mater.* **2020**, *10*, 2000022. [[CrossRef](#)]
77. Zhang, R.; Yan, K.; Palumbo, A.; Xu, J.; Fu, S.; Yang, E.H. A stretchable and bendable all-solid-state pseudocapacitor with dodecylbenzenesulfonate-doped polypyrrole-coated vertically aligned carbon nanotubes partially embedded in PDMS. *Nanotechnology* **2019**, *30*, 095401. [[CrossRef](#)]
78. Dubey, A.; Arora, A. Advancements in carbon capture technologies: A review. *J. Clean. Prod.* **2022**, *373*, 133932. [[CrossRef](#)]
79. Turgut, O.; Bjerketvedt, V.S.; Tomasgard, A.; Roussanaly, S. An integrated analysis of carbon capture and storage strategies for power and industry in Europe. *J. Clean. Prod.* **2021**, *329*, 129427. [[CrossRef](#)]
80. McLaughlin, H.; Littlefield, A.A.; Menefee, M.; Kinzer, A.; Hull, T.; Sovacool, B.K.; Bazilian, M.D.; Kim, J.; Griffiths, S. Carbon capture utilization and storage in review: Sociotechnical implications for a carbon reliant world. *Renew. Sustain. Energy Rev.* **2023**, *177*, 113215. [[CrossRef](#)]
81. Kotagodahetti, R.; Hewage, K.; Karunathilake, H.; Sadiq, R. Long-term feasibility of carbon capturing in community energy systems: A system dynamics-based evaluation. *J. Clean. Prod.* **2022**, *377*, 134460. [[CrossRef](#)]
82. Hsan, N.; Dutta, P.K.; Kumar, S.; Das, N.; Koh, J. Capture and chemical fixation of carbon dioxide by chitosan grafted multi-walled carbon nanotubes. *J. CO₂ Util.* **2020**, *41*, 101237. [[CrossRef](#)]
83. Lee, J.W.; Kim, M.; Jung, H.S.; Xu, R.; Kim, S.; Kang, Y.T. Liquid-like adsorbent assembled by CNTs: Serving as renewable CO₂ capture materials for indoor air. *J. Energy Chem.* **2021**, *63*, 574–584. [[CrossRef](#)]
84. Lee, J.W.; Kim, M.; Park, J.H.; Kang, Y.T. Recyclable carbon nanotube/silicone oil emulsion with NaOH aqueous solution for indoor CO₂ capture. *Green Chem.* **2022**, *24*, 6264–6277. [[CrossRef](#)]
85. Kim, S.; Han, J.; Choi, J.M.; Nam, J.S.; Lee, I.H.; Lee, Y.; Novikov, I.V.; Kauppinen, E.I.; Lee, K.; Jeon, I. Aerosol-Synthesized Surfactant-Free Single-Walled Carbon Nanotube-Based NO₂ Sensors: Unprecedentedly High Sensitivity and Fast Recovery. *Adv. Mater.* **2024**, *36*, 2313830. [[CrossRef](#)] [[PubMed](#)]
86. Kouediatouka, A.N.; Wang, J.; Mawignon, F.J.; Wang, W.; Liu, Q.; Meng, Z.; Makanda, I.L.D.; Djandja, O.S.; Dong, G. Carbon nanotube/liquid metal hybrid coating-based flexible pressure piezoresistive sensors. *Chem. Eng. J.* **2024**, *481*, 148637. [[CrossRef](#)]
87. Feng, X.; Li, P.; Li, T.; Cao, X.; Liu, D.; Xiao, M.; Wang, L. Ultra-sensitive and rapid detection of *Salmonella enterica* and *Staphylococcus aureus* to single-cell level by aptamer-functionalized carbon nanotube field-effect transistor biosensors. *Biosens. Bioelectron.* **2024**, *257*, 116333. [[CrossRef](#)]

Disclaimer/Publisher’s Note: The statements, opinions and data contained in all publications are solely those of the individual author(s) and contributor(s) and not of MDPI and/or the editor(s). MDPI and/or the editor(s) disclaim responsibility for any injury to people or property resulting from any ideas, methods, instructions or products referred to in the content.